A Real-Time Edge-Preserving Denoising Filter

Simon Reich[1], Florentin Wörgötter[1], and Babette Dellen[2]
[1] *Third Institute of Physics - Biophysics, Georg-August-Universität Göttingen, Friedrich-Hund-Platz 1, 37077 Göttingen, Germany*
[2] *Hochschule Koblenz, Joseph-Rovan-Allee 2, 53424 Remagen*
{sreich, worgott}@gwdg.de, dellen@hs-koblenz.de

Keywords: Edge-Preserving, Denoising, Real-Time

Abstract: Even in todays world, where augmented reality glasses and 3d sensors become rapidly less expensive and widely more used, the most important sensor remains the 2d RGB camera. Every camera is an optical device and prone to sensor noise, especially in dark environments or environments with extreme high dynamic range. The here introduced filter removes a wide variation of noise, for example Gaussian noise and salt-and-pepper noise, but preserves edges. Due to the highly parallel structure of the method, the implementation on a GPU runs in real-time, allowing us to process standard images within tens of milliseconds. The filter is first tested on 2d image data and based on the Berkeley Image Dataset and Coco Dataset we outperform other standard methods. Afterwards, we show a generalization to arbitrary dimensions using noisy low level sensor data. As a result the filter can be used not only for image enhancement, but also for noise reduction on sensors like acceleremoters, gyroscopes, or GPS-trackers, which are widely used in robotic applications.

1 INTRODUCTION

Real-time computer vision in fast moving robots still remains a challenging task, especially when forced to use limited computing power, as it is usually the case when implemented on embedded systems. Different light conditions are just one aspect of this vast field of problems. Cameras (analog as well as digital cameras) introduce noise in poor light conditions, meaning in environments with low signal-to-noise ratio.

Removing this noise usually leads to better performance of object recognition tasks in 2d and 3d images, more stable computation of features, and improve tracking results. It was shown (Reich et al., 2013) that removal of texture from 2d images significantly improves image segmentation results.

An additional application is the automatic production of images, which are, generally speaking, more appealing to humans; there is a big community of photographers and we deem removing noise for pure aesthetic value as also important. One application of the here presented filter is shown in Fig. 1.

Still, the filter generalizes well on arbitrary dimensions. In a second part we will show how to apply the same mechanisms to an arbitrary number of dimensions, enabling the filter to run on any physical measurement, for example on 1d sensor data obtained from an accelerometer, gyroscope, or GPS tracker.

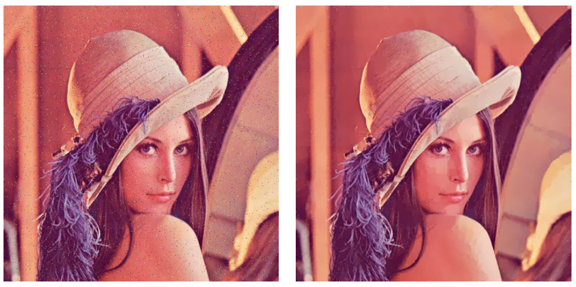
(a) Noisy test image. (b) Denoised test image.
Figure 1: Even today, denoising remains a challenging task. Here, we propose a novel, real-time denoising filter, which we call Edge-Preserfing-Filter (EPF).

Removing noise is a two-step process: First a noisy pixel needs to be detected, second it needs to be smoothed out. Both steps offer a wide range of problems. In the first step we need to define a noisy pixel in a mathematical sense, such that a computer can understand what we are looking for. This means that we will need to define a similarity criterion. However, similarities can exist on different scales, i.e. between adjacent pixels or groups of pixels, as it is the case for texture. In the second step a target value needs to be computed, which replaces the noisy pixel. This target value should, again, only depend on the local neighborhood.

Removing noise has a long history in science. Most notable is the Gaussian Filter. It works by convolving an image with a Gaussian function and thus works as a simple low-pass filter, attenuating high frequency signals (Gonzalez and Woods, 2002, p. 257f). As edges are also a high-frequency signal, they will be blurred out, too.

Noise in images is usually distinguished using a threshold. This thresholds can be either learned using a training set of images, as in support vector machines (Yang et al., 2010) and neural networks (Muneyasu et al., 1995; Pandey et al., 2016), or the threshold may be computed from the surrounding pixel values, as in (Du et al., 2011). (Lev et al., 1977) identified similar pixels by detecting edges and itertively replacing the intensity of the pixel by the mean of all pixels in a small environment.

Another approach is presented in (Tomasi and Manduchi, 1998): The so called bilateral filter blurs neighboring pixels depending on their combined color and spatial distance. Hence, texture and noise, which has small deviation from the mean can be blurred without affecting boundaries. This leads to a trade-off: large blurring factors are needed to smooth out high level of noise, having the consequence that edges are not preserved anymore.

Another wide class of algorithms denoise by averaging. This averaging may happen locally as in the Gaussian smoothing model (Lindenbaum et al., 1994), the anisotropic smoothing model (Perona and Malik, 1990; Alvarez et al., 1992), based on neighborhood filtering as in the already mentioned bilateral filter (Tomasi and Manduchi, 1998), using local variations as in (Rudin et al., 1992), or based on the wavelet thresholding method (Donoho, 1995).

All this powerful methods have one common drawback: they all smooth small scaled noise and preserve color edges, although however are not able to distinguish between a color edge and large scaled noise, e.g. outliers. Outliers are a common problem in any sensor based application, as in accelerometers or gyroscopes, but also in 2d-rgb cameras, where high ISO settings often pose a big problem. More recent methods, which achieve this goal (Dabov et al., 2007; Zoran and Weiss, 2011; Mairal et al., 2009), do not perform in real-time. The here presented approach has the following features: (1) smooths out small scaled noise, (2) smooths out outliers, (3) still preserves color edges, and (4) performs in real-time.

In the following section, we introduce a mathematical formulation of our filter in the discrete and continuous domain. Afterwards, we will utilize the algorithm using artificial noise on an image data sets and compare the results. Then, we describe the generalization on benchmark data and perform experiments on artificial data. This will be followed by a detailed discussion and conclusion.

2 METHOD

Let $\Phi(i)$ be our observed image. Then our noisy image is defined as

$$\Phi(i) = u(i) + n(i), \tag{1}$$

where $u(i)$ is the "true" value and $n(i)$ is the noise at image position i. Here, we will model noise as Gaussian white noise, meaning $n(i)$ is Gaussian distributed with zero mean and variance σ^2. Additionally we will add salt-and-pepper noise: a fixed percentage of color channels will be set to either 0 or its maximum value. We define our filter D_h, with filter parameter h, as follows

$$\Phi = D_h(\Phi) + n \tag{2}$$

meaning, that for an optimal filter

$$u = D_h(u + n) \tag{3}$$

should be true. The filter parameter h should depend only on the variance of the noise $h = h(\sigma)$. Later, for evaluation the Root-Mean-Square Error (RMSE) and Peak Signal-to-Noise Ratio (PSNR) between u and $D_h(u+n)$ is computed.

2.1 Proposed Filter

A flowchart of the proposed filter is shown in Fig. 2. First, the image Φ is divided into subwindows Ψ sized $N = k \cdot l$, where each subwindow is shifted by one pixel relative to the last one, such that there are as many subwindows as there are pixels in the image. Each subwindow is then smoothed using a Gaussian kernel. Subwindow size $k \times l$ and Gaussian smoothing parameter are hyperparameters, which need to be manually set. However, all three heavily depend on the amount of noise you would want to remove. For each subwindow centered around pixel position (i, j) a distance matrix $\Delta_{i,j}$ and a mean distance $\delta^m_{i,j}$ is computed in the color domain. This offers a measurement for noise, as described below. A user selected threshold τ, which defines a threshold between noise and a mere color edge, is applied to $\Delta_{i,j}$ and $\delta^m_{i,j}$. In case of noise, a weight $\omega_{i,j}$ is computed, which will move the color values of the pixel in the subwindow to the mean color of the subwindow.

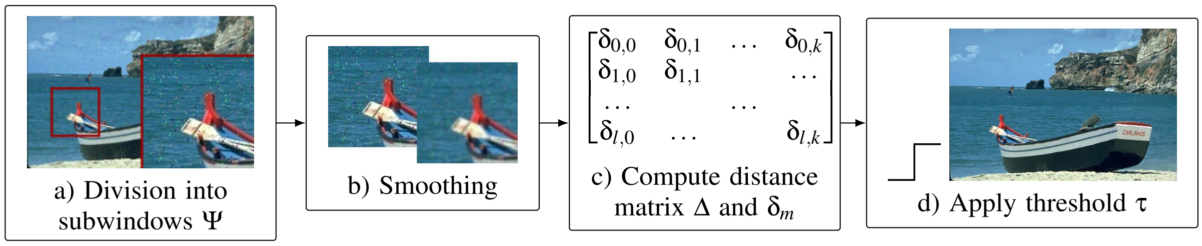
a) Division into subwindows Ψ
b) Smoothing
$\begin{bmatrix} \delta_{0,0} & \delta_{0,1} & \dots & \delta_{0,k} \\ \delta_{1,0} & \delta_{1,1} & & \dots \\ \dots & & \dots & \\ \delta_{l,0} & \dots & & \delta_{l,k} \end{bmatrix}$
c) Compute distance matrix Δ and δ_m
d) Apply threshold τ

Figure 2: Overview of the system structure. A detailed explanation of all steps is shown in section 2.

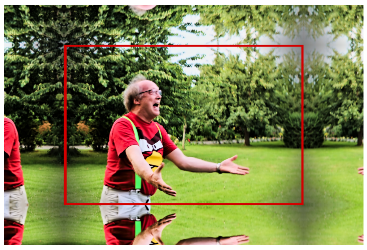

Figure 3: Peridiodic mirrored boundary conditions are used for image subwindows. Red rectangle denotes borders of original image.

Division into subwindows Let one pixel at position (i,j) contain the color information $\boldsymbol{\varphi}_{i,j} = (\varphi^r_{i,j}\ \varphi^g_{i,j}\ \varphi^b_{i,j})^T$. We create a subwindow $\Psi^{(i,j)}$ around (i,j), such that (i,j) is centered. In case we hit an image boundary, periodic mirrored boundary conditions are used as visualized in Fig. 3. The size of the subwindow is defined by $k \times l$ and pixel position inside the subwindow will be denoted by (r,s), such that $0 \leq r < k$ and $0 \leq s < l$.

Smoothing Each subwindow is smoothed via a Gaussian kernel (Gonzalez and Woods, 2002, p. 257f). This removes outliers, which would otherwise distort the computation of the mean as described in the next step.

Computation of the distance matrix For each subwindow $\Psi^{(i,j)}$ the arithmetic mean is calculated as

$$\boldsymbol{\psi}^{(i,j)}_m = \frac{1}{N} \left(\sum_{r,s} \psi^r_{r,s} \sum_{r,s} \psi^g_{r,s} \sum_{r,s} \psi^b_{r,s} \right)^T \tag{4}$$

where $N = k \cdot l$ denotes the size of the subwindow. The pixelwise distances

$$\delta^{(i,j)}_{r,s} = |\boldsymbol{\psi}_{r,s} - \boldsymbol{\psi}^{(i,j)}_m|_2 \tag{5}$$

are stored in a matrix $\Delta^{(i,j)}$. Furthermore, for each subwindow $\Psi^{(i,j)}$ the mean pixelwise distance

$$\delta^{(i,j)}_m = \frac{1}{N} \sum_{r,s} \delta^{(i,j)}_{r,s} \tag{6}$$

is calculated.

Thresholding Using a threshold we will now analyze, whether a subwindow contains a color edge (and therefore no pixels should be smoothed), one pixel contains an outlier (and should be corrected), or neither, which means the pixel value should also not be replaced. If $\delta^{(i,j)}_m$ is large, we have a subwindow with big color variations. This means we have found a subwindow, which holds a color edge. If $\delta^{(i,j)}_m$ is small, but one single pixel holds a big color variations (large $\delta^{(i,j)}_{r,s}$), we have found an outlier, which needs to be replaced. If both, $\delta^{(i,j)}_m$ and $\delta^{(i,j)}_{r,s}$ are small, the pixel holds a "normal color" value. We can now introduce a threshold τ to identify noisy pixels and color edges, yielding

$$\psi_{r,s} = \begin{cases} \text{color edge} & \text{, if } \delta^{(\mathrm{i,j})}_{\mathrm{m}} > \tau, \\ \text{noise} & \text{, if } \delta^{(\mathrm{i,j})}_{\mathrm{m}} \leq \tau \text{ and } \delta_{\mathrm{r,s}} > \tau, \\ \text{neither} & \text{, else.} \end{cases} \tag{7}$$

Update of RGB values A new image Θ, holding the pixel values $\boldsymbol{\theta}_{i,j}$ is computed based upon the squared distance of the user based threshold τ and the pixelwise distance $\delta_{r,s}$. $\boldsymbol{\theta}_{i,j}$ is updated as follows

$$\boldsymbol{\theta}_{i,j} \longleftarrow \boldsymbol{\theta}_{i,j} + \psi_{r,s} \cdot \left(\tau - \delta^{(i,j)}_{r,s}\right)^2 \cdot \boldsymbol{\psi}^{(i,j)}_m. \tag{8}$$

Please note, that due to the sliding subwindows each pixel is updated $N = k \cdot l$ times and therefore needs to be normalized. Thus, an additional weight Ω is introduced for each pixel $\omega_{i,j}$ as

$$\omega_{i,j} \longleftarrow \omega_{i,j} + \psi_{r,s} \cdot \left(\tau - \delta^{(i,j)}_{r,s}\right)^2. \tag{9}$$

The final image results from division of Θ by Ω. In rare cases $\tau = \delta^{(i,j)}_{r,s}$ for large image patches can happen, which will result in $\omega_{i,j} = 0$ according to (9). To avoid division by zero we suggest to initialize Ω with ones instead of zeros (since in general $\omega_{i,j} \gg 0$, this does not change the final outcome significantly).

An example for these subwindows can be seen in Fig. 4. For demonstration purposes a simple 1d grayscale image holding 100 pixels is shown. Each

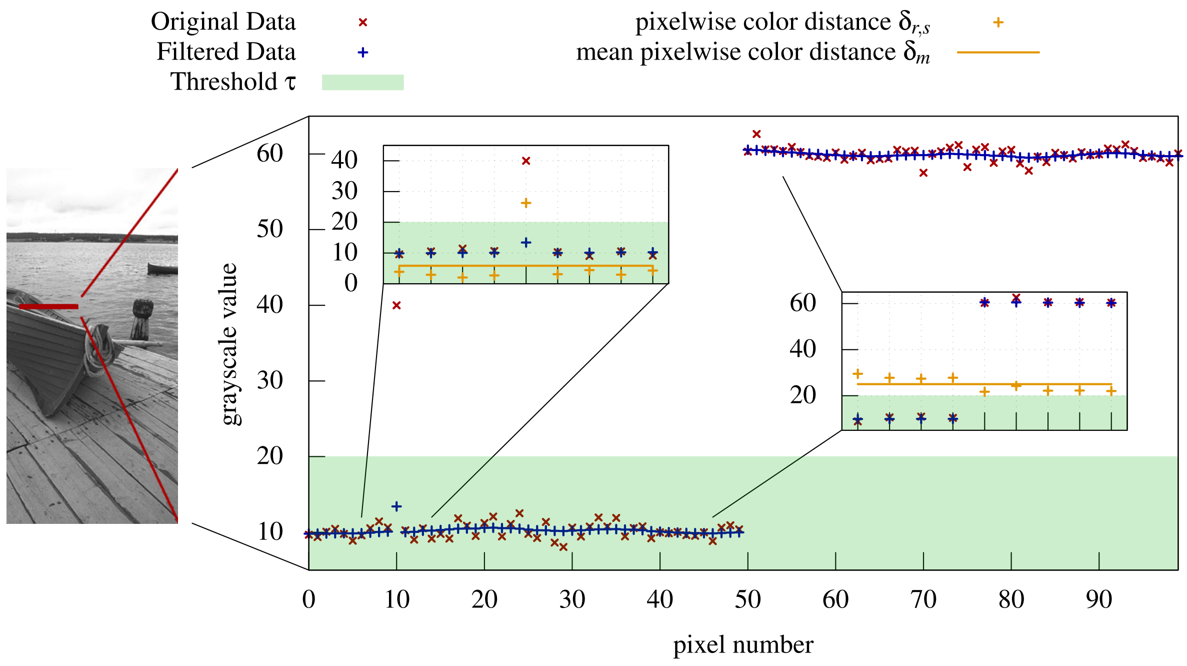

Figure 4: On the left a grayscale image, which needs to be filtered, is shown. For visualization purposes 100 px (marked in red) are chosen for detailed analysis and plotted in the large graph. Each pixel has Gaussian noise (variance of 1) added, additionally pixel 10 contains an outlier. At pixel 50 there is a color edge. In blue the same pixels are shown after being processed by the filter. The left subplot contains one subwindow sized 9×1 px. Pixel 10 is smoothed out, since the mean pixelwise color distance δ_m is low and thus pixel 10 is identified as noise. The right subgraph shows another subwindow, which detects of a color edge. δ_m is greater than threshold τ and therefore no values are smoothed inside this subwindow.

pixel has low variance Gaussian noise added. Pixel 10 was manually set to a significant higher value; at pixel 50 a color edge begins. Noisy pixel 10 is identified, since the mean pixelwise color distance δ_m is quiet low, while the pixelwise color distance $\delta_{r,s}$ is large; thus pixel 10 is smoothed out. At the color edge the mean pixelwise distance is greater than the threshold $\delta_m > \tau$, which is interpreted correctly as a color edge and thus no value in the shown subwindow is smoothed out.

However, one problem arises, when the subwindow contains only one pixel from the color edge. This one pixel cannot safely be differentiated between noise and color edge – even for a human this would be an impossible task. Therefore, pixels at the border of the subwindow are not smoothed, when detected as noise.

2.2 Formulation of the proposed filter in the continuous domain

Let $\boldsymbol{f}(\boldsymbol{x})$ define the smoothed input image, $\boldsymbol{h}(\boldsymbol{x})$ the output image, $\boldsymbol{c}(\boldsymbol{\zeta},\, \boldsymbol{x})$ measures the geometric closeness and $\boldsymbol{s}(\boldsymbol{f}(\boldsymbol{\zeta}),\, \boldsymbol{f}(\boldsymbol{x}))$ the photometric similarity. As we want to address specifically color images, bold letters refer to RGB-vectors. In this section $|\cdot|$ also refers to per-element-multiplication instead of vector multiplication. In our approach we first want to detect noise based on a user defined parameter τ. If noise is detected, we want to remove it, and in case of a color edge, we want to preserve the edge. Therefore, we define a mean value

$$\begin{aligned} \boldsymbol{m}(\boldsymbol{x}) &= \boldsymbol{k}_m^{-1}(\boldsymbol{x}) \int_{-\infty}^{\infty}\int_{-\infty}^{\infty} \boldsymbol{f}(\boldsymbol{\zeta}) \cdot \boldsymbol{c}(\boldsymbol{\zeta},\, \boldsymbol{x})\, \mathrm{d}\boldsymbol{\zeta} \\ \boldsymbol{k}_m(\boldsymbol{x}) &= \int_{-\infty}^{\infty}\int_{-\infty}^{\infty} \boldsymbol{c}(\boldsymbol{\zeta},\, \boldsymbol{x})\, \mathrm{d}\boldsymbol{\zeta} \end{aligned} \tag{10}$$

and a distance function

$$d\left(\boldsymbol{f}(\boldsymbol{x}),\, \boldsymbol{m}(\boldsymbol{x})\right) = \left|\boldsymbol{f}(\boldsymbol{x}) - \boldsymbol{m}(\boldsymbol{x})\right|, \tag{11}$$

which results in the pixelwise distance. The mean value $\boldsymbol{m}(\boldsymbol{x})$ now holds the average color value inside a spatial neighborhood of $\boldsymbol{x}$ and d holds the color distance from the pixel to the average $\boldsymbol{m}(\boldsymbol{x})$. If the spatial neighborhood holds only small scaled noise we expect a low pixelwise distance d, as well as a low average pixelwise distance in the spatial neighborhood $\boldsymbol{c}$:

$$\begin{aligned} p(\boldsymbol{x}) &= k_p^{-1} \iint_{-\infty}^{\infty} d\left(\boldsymbol{f}(\boldsymbol{\zeta}),\, \boldsymbol{m}(\boldsymbol{x})\right) \boldsymbol{c}(\boldsymbol{\zeta},\, \boldsymbol{x})\, \mathrm{d}\boldsymbol{\zeta} \\ k_p(\boldsymbol{x}) &= \iint_{-\infty}^{\infty} \boldsymbol{c}(\boldsymbol{\zeta},\, \boldsymbol{x})\, \mathrm{d}\boldsymbol{\zeta}. \end{aligned} \tag{12}$$

Therefore, we can make a decision using a threshold τ as

$$\boldsymbol{h}(\boldsymbol{x}) = \boldsymbol{k}_R^{-1}(\boldsymbol{x}) \cdot \begin{cases} \iint_{-\infty}^{\infty} \boldsymbol{f}(\boldsymbol{\zeta}) \cdot \boldsymbol{c}(\boldsymbol{\zeta},\, \boldsymbol{x}) \cdot \boldsymbol{s}(\boldsymbol{\zeta},\, \boldsymbol{x})\, \mathrm{d}\boldsymbol{\zeta} & p \leq \tau \\ \iint_{-\infty}^{\infty} \boldsymbol{f}(\boldsymbol{\zeta}) \cdot \boldsymbol{c}(\boldsymbol{\zeta},\, \boldsymbol{x}) \cdot \boldsymbol{s}(\boldsymbol{\zeta},\, \boldsymbol{x})\, \mathrm{d}\boldsymbol{\zeta} & p \leq \tau, d > \tau \\ \iint_{-\infty}^{\infty} \boldsymbol{f}(\boldsymbol{\zeta}) \cdot \boldsymbol{c}(\boldsymbol{\zeta},\, \boldsymbol{x})\, \mathrm{d}\boldsymbol{\zeta} & \text{else,} \end{cases}$$

where k_R is the respective normalization. d can now be used to distinguish large scale noise. We used a 2d step function

$$\boldsymbol{c}(\boldsymbol{\zeta},\, \boldsymbol{x}) = \begin{cases} 1 & \boldsymbol{x} - \boldsymbol{a} \leq \boldsymbol{\zeta} \leq \boldsymbol{x} + \boldsymbol{b} \\ 0 & \text{else} \end{cases}, \qquad (13)$$

using the conditions $\boldsymbol{a}, \boldsymbol{b}, \boldsymbol{e} \in \mathbb{R}^2_{\geq 0} | \boldsymbol{a} + \boldsymbol{b} = \boldsymbol{e}$ with a fixed $\boldsymbol{e}$. This generates a rectangle of the size $\boldsymbol{e}$ around $\boldsymbol{x}$. As this definition is not feasable in the continuous domain as it generates a nonfinite number of subwindows to calculte, in the discrete case however every pixel is checked and updated according to its neighborhood $\boldsymbol{e}$. As a measure for similarity we used a squared distance

$$\boldsymbol{s}((\boldsymbol{\zeta}),\, \boldsymbol{x}) = (\tau - d(\boldsymbol{f}(\boldsymbol{x}),\, \boldsymbol{m}(\boldsymbol{x})))^2 |\boldsymbol{m}(\boldsymbol{x})| \qquad (14)$$

and the euclidian norm. In case of noise detection the output is moved to the mean. The maximum size of the step can be adjusted via the threshold τ.

2.3 Real-time Implementation

The proposed filter can only run in real-time on parallel hardware, since the computation of multiple subwindows is very intensive on traditional CPUs. Still, once the image Φ is read, values for the subwindows $\Psi^{(i,j)}$ can be computed independently. For acceleration we use a graphics processor unit (GPU).

In our approach the images are filtered using a subwindow of size $k, l = 10$. As Δ and $\delta_m^{(i,j)}$ are calculated over each subwindow, this also sets the maximum size of noise that is detected. We tested two implementations of the algorithm: The CPU measurement refers to a single-threaded implementation using an Intel i7-3930K twelve-core processor at 3,2 GHz using one core and 16 GB RAM. The GPU version is executed on an Nvidia GTX580 graphics card using 512 cores and 1.5 GB device memory.

3 EXPERIMENTS

In this section, we will first look at the user controlled parameters, the subwindow size N and the threshold τ. The Gaussian smoothing parameters, which are also hyperparameters, heavily depend on the data type: is the filter too strong, the final image will be blurry; a filter too weak will not smooth enough. We found a kernel size of 5 px and $\sigma = 0.3$ working very well for all images in the datasets. Afterwards, we will compare our proposed filter to the bilateral filter, simple Gaussian kernel, Median filter, and Non-local-means filter. Lastly, we will look into the computational complexity and real-time implementations.

3.1 Subwindow Size

First, we will have a look at the effect of the most imporant user controlled parameter: the size of the subwindow N. Since each pixel is N times checked, the computational complexity increases linearly with N. This parameter also controls the amount of noise, which is either classified as noise or color edge. In Fig. 5 a one dimensional grayscale image is shown and filtered using three different subwindow sizes $N = 3, 9, 15$ px. For each size the color edge is preserved. For $N = 3$ px, Fig. 5a, the filter follows the data more closely; this also means that an outlier, as shown in pixel 10 in the data sample, has a greater influence on the filtered data. For a subwindow size of $N = 9$ px, see Fig. 5b, the data is more heavily smoothed and the outlier is almost not visible in the filtered data. In Fig. 5c a subwindow size of $N = 29$ px was chosen. Since the color edge begins at pixel 26, it will be alwasy present in all subwindows of all left sided pixels due to the periodic boundary conditions. Additionally, the outlier on the left side increases the mean pixelwise distance, such that the left side is almost not smoothed at all. Only the right side, which does not contain the artificial outlier, is smoothed.

Thus, the subwindow controls the spatial size of a color edge to be detected.

3.2 Threshold τ

Next, we will analyze the effect of the threshold τ, this is depicted in Fig. 6. As shown in section 2, τ controls the maximum step size for detecting noise and color edges. In Fig. 6a a threshold of $\tau = 10$ is used, which is small enough to detect the color step. A larger threshold of $\tau = 15$, used in Fig. 6b, already introduces some smoothing at the color edge. Please also note, that the outlier pixel at position 10 is not any more detected as noise; instead it has significant effect on the smoothing of its neighboring pixels. A large threshold of $\tau = 30$ can be seen in Fig. 6c; 30 is by far bigger than any data point and consequently everything will be smoothed. The color edge is not preserved any more.

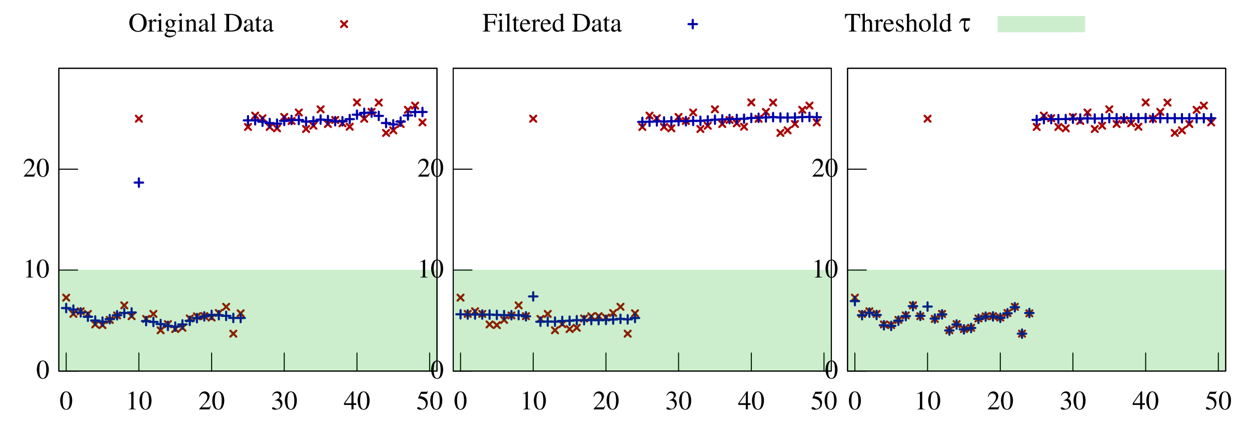

(a) Subwindow size of $N = 3$ px. (b) Subwindow size of $N = 9$ px. (c) Subwindow size of $N = 29$ px.

Figure 5: Shown is the effect of different subwindow sizes on one data set: a one dimensional grayscale image containing a color edge at pixel 25 and one outlier at pixel 10. In Fig. 5a a subwindow size of 3 px is shown. The data is smoothed and the color edge is preserved. The oulier at pixel 10, however, is also smoothed, but has also some effect on the neighboring pixels. A subwindow size of 9 px, as shown in Fig. 5b, seems to be more fitting: the outlier is smoothed and the color edge preserved. Fig. 5c shows a subwindow size of 29 px. The data on the left side is not smoothed, since the color edge and the outlier are always in one subwindow and thus the mean pixelwise color distance is greater than the threshold τ. This means the left side is always detected as “containing a color edge”. The right side of the data is smoothed, due to the periodic boundary conditions.

Thus, the threshold τ controls the maximum height of a color edge to be detected.

3.3 Application to 2D images

We corrupted our images by first adding Gaussian distributed noise to each pixel and each color channel using a standard deviation of $\sigma_c = 5$. Additionally, we added salt-and-pepper noise (s&p noise) to one color channel of 4% of all pixels. We tested on the Berkeley Segmentation Dataset and Benchmark (Arbelaez et al., 2011) (500 images) and the 2014 testing set of the Common Objects in Context Dataset (Coco Dataset) (Lin et al., 2014) (40775 images).

The corrupted image is then given to a simple Gaussian blurring filter (kernel size: 5×5 px, $\sigma_{x,y} = 2$), a bilateral filter ($\sigma_c = 110$, $\sigma_s = 5$) (Tomasi and Manduchi, 1998), a median blurring filter (kernel size: 3 px) (Sonka et al., 2014, p. 129f), a non-local-means filter ($h_d = 7$ px, $h_c = 7$ px, template window: 7×7 px, search window: 21×21 px) (Buades et al., 2005), and our proposed filter (subwindow: image size divided by 150, but at least 10×10 px, threshold $\tau = 10$). The denoised image is compared to the uncorrupted image using root-mean-square error (RMSE), defined as

$$\mathrm{RMSE} = \sqrt{\frac{\sum_{i=1}^{n} \left(\phi_{original} - \phi_{denoised}\right)^2}{n}}, \qquad (15)$$

Table 1: Comparison of RMSE and PSNR computed on the Berkeley Dataset (500 images) and the Coco Dataset (40775 images). The first line “Original” refers to the not denoised image. The last digits are uncertain due to rounding errors.

	Berkeley Dataset		Coco Dataset	
	RMSE	PSNR	RMSE	PSNR
Original	17.9(5)	23.3(1)	17.3(1)	23.3(3)
EPF	**7.0(6)**	**31.0(5)**	**7.8(9)**	**30.4(7)**
Bilateral	10.4(1)	27.7(5)	10.4(3)	28.0(1)
Gaussian	14.5(9)	25.0(8)	15.6(9)	24.8(1)
Median	14.0(4)	25.6(3)	14.9(1)	25.5(4)
NLM	11.4(0)	26.8(6)	12.2(8)	26.4(4)

and peak signal-to-noise ratio (PSNR):

$$\mathrm{PSNR} = 20 \cdot \log_{10}\left(\frac{\max(\phi_{original})}{\mathrm{RMSE}}\right). \qquad (16)$$

All filter parameters listed above were chosen to minimize RMSE and maximize PSNR. Results are shown in Tab. 1 and will be discussed in the next section. Image examples are provided in figure 7.

The proposed filter achieves on both datasets the best performance markers. In the discussion, section 4, we will compare our results to more recent, state-of-the art algorithms.

3.4 Application to 1D sensor data

As already suggested in Fig. 4, 5, and 6, the filter can also be applied to 1D data. This may happen, for exam-

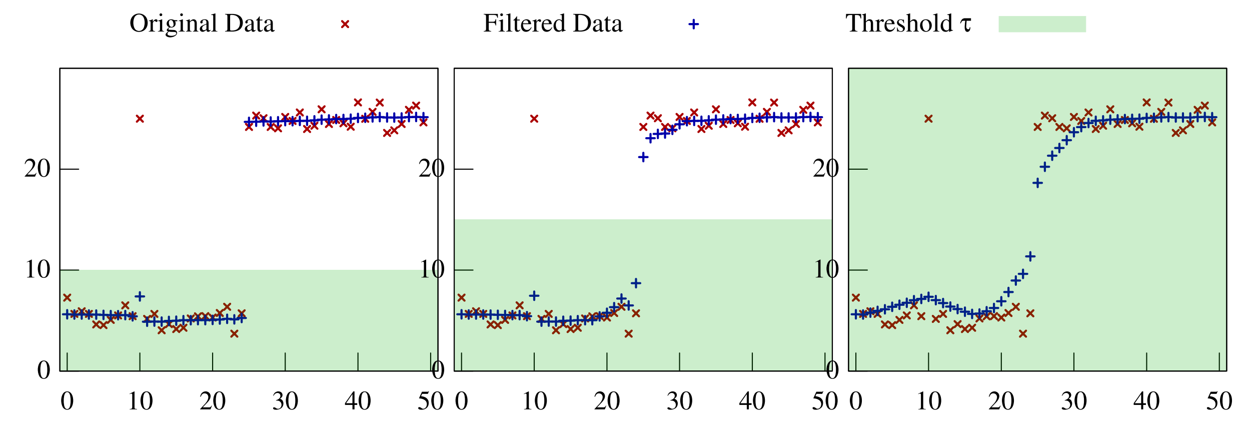

(a) Threshold of $\tau = 10$. (b) Threshold of $\tau = 15$. (c) Threshold of $\tau = 30$.

Figure 6: Shown is the effect of three different thresholds on one data set: a one dimensional grayscale image containing a color edge at pixel 25 and one outlier at pixel 10. The subwindow size is $N = 9\,\text{px}$. In Fig. 6a a threshold of $\tau = 10$ is used. The outlier is detected as such and smoothed and the color edge is preserved. In Fig. 6b, however, the outlier at pixel 10 is not detected as such; it raises the average pixel value of the subwindows and has great influence on the smoothing: all pixels in its local neighborhood have an increased value after smoothing. Also the color edge is not preserved any more. This effect becomes even more visible in Fig. 6c, where heavy smoothing is applied to the color edge.

ple, as a post-processing step for sensor readings. We have tested the filter on three different settings: first, an alternating line, which switches every 100 samples its height to either $f(x) = f_{min}$ or $f(x) = f_{max}$; second, a sawtooth wave defined by $f(x) = x - \text{floor}_{100}(x)$l; and third, a sinusoidal wave $f(x) = \sin 2\pi x/250$ with a wave length of 250 data points. Every data line consists of a total length of 1000 samples. To each scenario either Gaussian noise with variance of $\sigma = 10$, salt-and-pepper noise (to 5% of samples), or both is added.

Again, we compared our proposed filter ($N = 11$, $\tau = 30$) to a Gaussian blurring filter (kernel: $7 \times 7\,\text{px}$, $\sigma_{x,y} = 3$), a bilateral filter ($\sigma_c = 30$, $\sigma_s = 30$, and a median filter (kernel size: 9 px). We computed RMSE and PSNR according to (15) and (16). Results are shown in Tab. 2.

In almost all experiments we outperform other standard 1d filtering methods. While the median filter performs very well on salt-and-pepper noise, it is not edge preserving and thus introduces artefacts on edges. The bilateral filter on the other hand, handles edges very well, but has significant trouble with removing salt-and-pepper noise. Our proposed EPF filter performs well on both, Gaussian and salt-and-pepper noise and is edge preserving.

3.5 Time Performance Results

We computed the average frame rates for differently sized images in Tab. 3. 100 images from the validation data set from (Arbelaez et al., 2011) were used and the results averaged. As shown in section 2 the computational complexity does not depend on the threshold and rather increases linearly with frame and subwindow size. In this test, a subwindow size of $10 \times 10\,\text{px}$ is used. Results are shown in Tab. 3. The GPU implementation for all frame sizes is about 40 times faster than the CPU implementation. However, our CPU implementation is rather naive and still open for improvements. For images of size $480 \times 320\,\text{px}$ real-time performance of movies is achieved.

4 DISCUSSION AND CONCLUSION

In this paper, we presented a novel real-time edge preserving smoothing filter, which replaces noisy areas by uniformly colored patches. Performance is significantly better than other standard methods on 2d images. Artificial 1d data shows similar results.

In (Gu et al., 2014) a comparison to other methods is given, including state-of-the-art methods like BM3D (Dabov et al., 2007), EPLL (Zoran and Weiss, 2011), or LSSC (Mairal et al., 2009) based on the Berkeley Dataset. All these methods exploit the image nonlocal redundancies, in contrast to our method, which uses a local neighborhood. In Tab. 4 a comparison between our proposed EPF filter and other state-of-the-art methods is shown. Clearly, our proposed method performs slightly worse than other recent algorithms. On the contrary the review (Shao et al., 2014) performs a con-

Table 2: Comparison of RMSE and PSNR computed on three different scenes: 1) an alternating line, 2) a sawtooth wave, and 3) a sinusoidal wave. To each scene three different noises (Gaussian (G.), salt-and-pepper (s&p), or both) is added, resulting in 9 different experiments. Each experiment is repeated 1000 times and averaged.

		Gauss		s&p		Gauss and s&p	
		RMSE	PSNR	RMSE	PSNR	RMSE	PSNR
	No denoising	10.0	22.3	15.2	16.4	18.1	17.2
1) Alternating Line	EPF	**2.6**	**32.3**	**3.9**	**28.5**	**5.1**	**26.7**
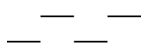	Bilateral	6.9	25.3	15.2	16.4	16.5	17.7
	Gaussian	6.0	25.3	7.8	22.2	8.7	22.1
	Median	5.1	26.8	4.1	27.9	6.0	25.4
	No denoising	10.0	21.6	14.1	17.1	17.1	17.0
2) Sawtooth Wave	EPF	**3.7**	**29.3**	**4.6**	**26.5**	**6.6**	**24.5**
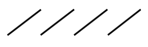	Bilateral	7.0	24.4	14.0	17.1	15.5	17.5
	Gaussian	7.6	22.6	8.8	20.9	9.6	20.6
	Median	5.7	25.2	5.8	24.9	7.4	23.1
	No denoising	10.0	20.1	12.9	17.8	16.1	16.0
3) Sinusoidal Wave	EPF	**2.7**	**29.5**	2.6	29.8	**4.4**	**25.6**
	Bilateral	6.7	23.0	12.8	17.9	14.4	16.9
	Gaussian	3.9	26.7	5.0	24.2	6.3	22.6
	Median	4.1	26.1	**0.6**	**46.1**	4.5	25.6

Table 3: Time performance for images of different sizes. The test images were taken from the validation set of the Berkeley Segmentation Dataset and Benchmark (Arbelaez et al., 2011). 100 measurements were taken and averaged. Our proposed EPF filter is compared to state-of-the-art algorithm BM3D (Dabov et al., 2007) as shown in (Shao et al., 2014). BM3D is, according to (Shao et al., 2014), one of the fastest recent methods.

Image Size [px]	CPU [Hz]	GPU [Hz]	BM3D [Hz]
240×180	2.0	80.4	
320×240	1.1	48.0	
480×320	0.5	23.8	0.4
640×480	0.3	12.4	
800×600	0.2	7.7	0.1
1024×768	0.1	4.2	0.1

clusive study on computational complexity. According to this work of the fastest algorithms, BM3D, manages to denoise not more than one image sized 256×256 px per second. This is far from real-time and not feasable for robotic applications or critical sensor readings. A comparison to the proposed EPF filter is shown in Tab. 3.

This means, our system performs only slightly worse than recent denoising methods, but offers real-time performance, which makes the filter applicable to video streams and hence can be used in the future as a component inside the perception-action loop of robotic applications. It enables image processing and data filtering on embedded hardware, for example in flying robots, which is another research area of ours. The filter not only works well in the image domain, but can be extended to data of any dimension, e.g. noisy 6d point cloud data. In our work we demonstrated this by filtering 1d sensor data. This work will be submitted to the opencv image library (Bradski, 2000) to enable easy usage and comparison to other methods.

Table 4: PSNR values for state-of-the-art methods (as shown in (Gu et al., 2014)) compared to our proposed EPF filter.

Gaussian Noise	Recent Methods	EPF
$\sigma = 10$	$33.5 - 34.8$	30.7
$\sigma = 30$	$27.8 - 29.2$	23.0
$\sigma = 50$	$25.1 - 26.8$	19.9
$\sigma = 100$	$21.6 - 23.6$	15.5

ACKNOWLEDGEMENTS

The research leading to these results has received funding from the European Communitys H2020 Programme under grant agreement no. 680431, ReconCell.

REFERENCES

Alvarez, L., Lions, P.-L., and Morel, J.-M. (1992). Image selective smoothing and edge detection by nonlinear diffusion. ii. *SIAM Journal on numerical analysis*, 29(3):845–866.

Arbelaez, P., Maire, M., Fowlkes, C., and Malik, J. (2011). Contour detection and hierarchical image segmentation. *IEEE transactions on pattern analysis and machine intelligence*, 33(5):898–916.

Bradski, G. (2000). Opencv. *Dr. Dobb's Journal of Software Tools*.

Buades, A., Coll, B., and Morel, J.-M. (2005). A non-local algorithm for image denoising. In *IEEE Conference on Computer Vision and Pattern Recognition(CVPR)*, volume 2, pages 60–65. IEEE.

Dabov, K., Foi, A., Katkovnik, V., and Egiazarian, K. (2007). Image denoising by sparse 3-d transform-domain collaborative filtering. *IEEE Transactions on image processing*, 16(8):2080–2095.

Donoho, D. L. (1995). De-noising by soft-thresholding. *IEEE transactions on information theory*, 41(3):613–627.

Du, W., Tian, X., and Sun, Y. (2011). A dynamic threshold edge-preserving smoothing segmentation algorithm for anterior chamber oct images based on modified histogram. In *4th International Congress on Image and Signal Processing (CISP)*, volume 2, pages 1123–1126. IEEE.

Gonzalez, R. C. and Woods, R. E. (2002). *Digital image processing*. Pearson Prentice Hall.

Gu, S., Zhang, L., Zuo, W., and Feng, X. (2014). Weighted nuclear norm minimization with application to image denoising. In *Proceedings of the IEEE Conference on Computer Vision and Pattern Recognition*, pages 2862–2869.

Lev, A., Zucker, S. W., and Rosenfeld, A. (1977). Iterative enhancemnent of noisy images. *IEEE Transactions on Systems, Man, and Cybernetics*, 7(6):435–442.

Lin, T.-Y., Maire, M., Belongie, S., Hays, J., Perona, P., Ramanan, D., Dollár, P., and Zitnick, C. L. (2014). Microsoft coco: Common objects in context. In *European Conference on Computer Vision*, pages 740–755. Springer.

Lindenbaum, M., Fischer, M., and Bruckstein, A. (1994). On gabor's contribution to image enhancement. *Pattern Recognition*, 27(1):1–8.

Mairal, J., Bach, F., Ponce, J., Sapiro, G., and Zisserman, A. (2009). Non-local sparse models for image restoration. In *IEEE 12th International Conference on Computer Vision*, pages 2272–2279. IEEE.

Muneyasu, M., Maeda, T., Yako, T., and Hinamoto, T. (1995). A realization of edge-preserving smoothing filters using layered neural networks. In *IEEE International Conference on Neural Networks*, volume 4, pages 1903–1906. IEEE.

Pandey, M., Bhatia, M., and Bansal, A. (2016). An anatomization of noise removal techniques on medical images. In *International Conference on Innovation and Challenges in Cyber Security (ICICCS-INBUSH)*, pages 224–229.

Perona, P. and Malik, J. (1990). Scale-space and edge detection using anisotropic diffusion. *IEEE Transactions on pattern analysis and machine intelligence*, 12(7):629–639.

Reich, S., Abramov, A., Papon, J., Wörgötter, F., and Dellen, B. (2013). A novel real-time edge-preserving smoothing filter. In *International Conference on Computer Vision Theory and Applications*, pages 5 – 14.

Rudin, L. I., Osher, S., and Fatemi, E. (1992). Nonlinear total variation based noise removal algorithms. *Physica D: Nonlinear Phenomena*, 60(1):259–268.

Shao, L., Yan, R., Li, X., and Liu, Y. (2014). From heuristic optimization to dictionary learning: A review and comprehensive comparison of image denoising algorithms. *IEEE Transactions on Cybernetics*, 44(7):1001–1013.

Sonka, M., Hlavac, V., and Boyle, R. (2014). *Image processing, analysis, and machine vision*. Cengage Learning.

Tomasi, C. and Manduchi, R. (1998). Bilateral filtering for gray and color images. In *Sixth International Conference on Computer Vision*, pages 839–846. IEEE.

Yang, Q., Wang, S., and Ahuja, N. (2010). Svm for edge-preserving filtering. In *IEEE Conference on Computer Vision and Pattern Recognition (CVPR)*, pages 1775–1782. IEEE.

Zoran, D. and Weiss, Y. (2011). From learning models of natural image patches to whole image restoration. In *IEEE International Conference on Computer Vision (ICCV)*, pages 479–486. IEEE.

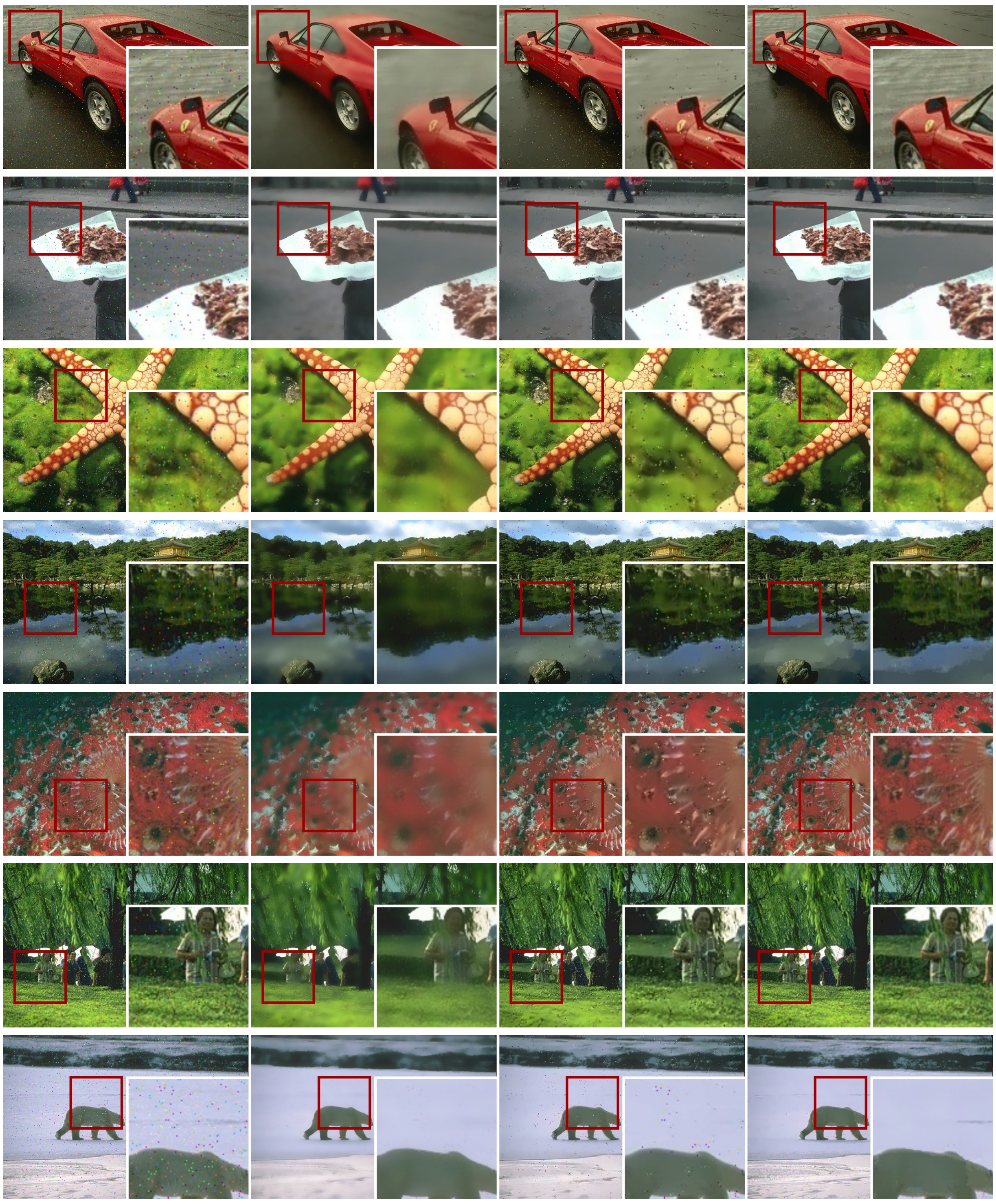

(a) Noisy test image. (b) Bilateral Filter. (c) Non-Local-Means Filter. (d) Proposed Filter.

Figure 7: Visual comparison of filter results. Quantitative results are shown in Tab. 1. Images taken from Berkeley Image Dataset (Arbelaez et al., 2011).